Chapter

Sorption of Phosphorus, Nickel, and Lead from Aqueous Solution Using Manganese Oxide-Coated Materials

Nesrine Boujelben

Abstract

Manganese oxide-coated sand (MOCS) and manganese oxide-coated crushed brick (MOCB) were prepared and characterized and employed for the removal of phosphorus ions (PO_4^{3-}) and Pb(II) and Ni(II) ions from aqueous solution. To study the surface properties of the adsorbents, scanning electron microscopy (SEM), X-ray diffraction (XRD) methods, and BET analyses were used. Adsorption was investigated by batch experiments. The estimated optimum pH was 7 for Ni(II) and 5 for all other ions retention by the two considered adsorbents. Both the Freundlich and Langmuir isotherms provided a reasonable fit to the experimental data for the adsorption. The adsorption capacities of the coated adsorbents at a considered pH value and a temperature of 20°C were 1.96 and 2.08 mg/g for PO_4^{3-}, 2.4 and 3.33 mg/g for Ni(II), and 6 and 6.25 for Pb(II) onto MOCS and MOCB, respectively. The pseudo-first-order and pseudo-second-order equations as well as the intraparticle diffusion model were determined to test the adsorption kinetics and the rate constants derived from the three kinetic models being calculated. The pseudo-second-order kinetic model was better appropriated. Results obtained from this study confirm that the manganese oxide-coated sorbent is considerably considered like suitable for the removal of anions and cations from aqueous solutions.

Keywords: manganese oxide-coated sorbents, nickel copper and lead removal, phosphorus ions, kinetic study, thermodynamic parameters

1. Introduction

Due to the rapid development of such industries as plating, petrochemicals, and fertilizers, there has been excessive discharge of contaminant, like phosphorus and heavy metals, into the environment, resulting in health hazards [1]. Phosphorus is the key nutrient for the growth of algal and other biological organisms, which in excess causes eutrophication of water bodies and heavy metals such as lead and nickel, which are harmful and can cause disease and damage to human health if present above certain concentrations [2, 3]. For this reason, it is important to remove them from wastewater before it is discharged into the environment [2]. There are many methods to eliminate heavy metals from wastewater [2], including chemical precipitation [4], electrochemical reduction [5], ion exchange [6],

membrane separation, reverse osmosis [7], and adsorption [8–10]. Adsorption is considered the most effective one due to its properties of simple operation, low cost, and high efficiency over a wide concentration range of pollutants [11]. Typical adsorbents which have been extensively employed to remove heavy metals are clay minerals [12], carbon-based materials [13], and metal oxides [14]. Recently, different types of low-cost natural and modified minerals for the removal of heavy metals from aqueous solutions have been used. Due to the high surface charge density, various Mn oxides (e.g., including pyrolusite (β-MnO_2) and birnessite (σ-MnO_2)) have been extensive as high efficient adsorbents to remove arsenic [15], nickel [16], and lead [17], for example.

Recent studies have shown that some filtration materials such as sand and burned clay coated with oxides (oxyhydroxides) of iron, aluminum, or manganese act as good and inexpensive sorbents [18–21].

In the present study, the characteristics of two prepared coated adsorbents, namely, manganese oxide-coated sand and manganese oxide-coated crushed brick, have been investigated.

Thermodynamic and kinetic studies of phosphorus ions (PO_4^{3-}) and Pb(II) and Ni(II) ions from aqueous solution adsorption onto these materials were also undertaken. The main objectives of this investigation were to examine quantitatively the effect of contact time, pH, and concentration on the removal of phosphorus ions (PO_4^{3-}) and Pb(II) and Ni(II) ions from aqueous solutions as well as to check in detail the kinetics of the phosphorus ions (PO_4^{3-}) and Pb(II) and Ni(II) ions from aqueous solution and ion-removal process.

2. Materials and methods

2.1 Sample preparation

In our previous works [20, 21], the average diameter for sand and crushed brick grains was 0.6–0.7 and 0.9–1.2 mm, respectively [20, 21], and the specific gravities were 2.50 and 2.39 g/cm^3 for sand and crushed brick, respectively [20, 21].

The manganese oxide-coated adsorbents (MOCS, sand, and MOCB, crushed brick) were prepared by impregnation according to the procedure proposed by Bajpai and Chaudhuri and adopted in our previous research work [20–22].

Before MnO_2 impregnation, an acidic purification procedure (acid wash with 1 M HCl) [20, 21, 23] was made to the adsorbents to remove impurities, which could affect the adsorption results. The reaction of $KMnO_4$ with hot $MnCl_2$ solution (48–50°C) under alkaline conditions (pH 9) over a period of 48 h [20] was the favorable conditions to ensure the application of the MnO_2 coating on the two adsorbent surfaces.

2.2 Chemicals

To prepare aqueous solutions containing phosphates and metal ions at various concentrations, sodium phosphate salt (NaH_2PO_4), lead nitrate salt [$Pb(NO_3)_2$], and nickel chloride salt ($NiCl_2$_$6H_2O$, analytical grade) solutions were used. The initial pH values of the solutions were adjusted by adding either nitric acid or sodium hydroxide solution [20, 21].

All chemicals used for the pre-treatment of the adsorbents, as well as for the adsorption tests, were of analytical grade (HCl, $MnCl_2$, $KMnO_4$, NaOH, HNO_3).

A calibrated pH meter (model pH 540 GLP) equipped with a combined glass electrode (SENTIX 41) [20, 21] was used to ensure the measurements of pH.

2.3 Sorbent characterization

X-ray diffractometer (Siemens, Germany) with Cu Kα radiation (λ = 0.154 nm) was used to determine the mineralogy of the manganese oxide-coating sorbents. The single-point BET (N_2) adsorption procedure was employed to characterize the specific surface area (m^2/g) of each adsorbent before and after coating [20, 21].

The pH of the point of zero charge (pHpzc) was determined by adding 0.1 g of adsorbent to a series of bottles that contained 50 ml of deionizer water. The pH of each solution was adjusted in the range of 1.0–9.0 by the addition of either 0.1 M HNO_3 or 0.1 M NaOH solutions. The bottles were then rotated for 1 h in a shaker and the pH values of the contents measured at the end of the test. The pH values of the suspensions were plotted as a function of the initial pH of the solutions, the resulting curve theoretically crossing the bisector of the axes at the point of zero charge [20, 21]. It is to note that the pHpzc values of 4.5 and 4.3 were obtained for MOCS and MOCB, respectively.

Philips XL 30 scanning electron microscope (SEM) was used to describe the morphology of the adsorbents before and after coating, and elemental spectra were obtained using energy-dispersive X-ray spectroscopy during the SEM observations [20, 21].

2.4 Adsorption experiments

The two prepared materials were first used in batch experiments to check the effect of the initial metal ion concentration on the adsorption kinetics and the influence of the initial pH. Five grams of manganese oxide-coated sorbent was added to 250 ml of each ion solution of known initial concentration [20, 21] and was used for the kinetic studies. The initial pH was adjusted to 5 with dilute HNO_3 or NaOH solution. Prepared solutions were shaken continuously for 4 h at the desired temperature (10, 20, and 40°C). This experiment was released by using a thermostatically controlled shaking water bath. Samples were taken at various time intervals and were immediately vacuum-filtered through a 0.45-μm membrane filter [20, 21].

Atomic absorption spectrophotometry (Hitachi Z-6100) was used to determine the residual ion concentration in each filtrate. Five percent was estimated to be the analytical errors. To ensure the veracity of the experimental results, all experiments were duplicated [20, 21].

To understand the influence of pH on the considered ion adsorption, experiments were performed at various initial pH values within the range 2–7 with the initial Pb(II) ion concentration being maintained at 50 mg/l and from 2 to 11 for Ni(II) and PO_4^{3-} ions. For each test, 1 g of sorbent was added to 25 ml of all considered ion solution, with the suspensions being shaken for 4 h at 20 ± 1°C [20, 21].

2.5 Adsorption isotherms

2.5.1 Isotherm determination

Experiments were conducted at 10°C, 20°C, and 40°C, respectively. At each temperature, 5 g of sorbent were contacted for 4 h with 250 ml of ion solution of different initial concentration [20, 21]. The adsorption equilibrium data were analyzed in terms of the Langmuir and Freundlich isotherm models. The linear forms of the Langmuir and Freundlich isotherms [24] may be expressed, respectively, by the following equations [20, 21]:

$$Ce/qe = 1/q_0b + Ce/q_0 \quad (1)$$

$$\log q_e = \log K_F + \frac{1}{n} \log C_e \quad (2)$$

where the Langmuir isotherm constants are q_0 (mmol/g) and b (g/mmol) and the Freundlich isotherm constants are K_F and n. The measure of the adsorption capacity of the sorbent value is q_0 (maximum amount of ions adsorbed at the temperature under consideration) [20, 21].

2.5.2 Determination of thermodynamic adsorption parameters

The standard Gibbs free energy (ΔG^0), the standard enthalpy (ΔH^0), and the standard entropy (ΔS^0) were determined to explain the effect of temperature on the adsorption parameters. It is known that the adsorption of metal ions is a reversible process corresponding to a heterogeneous equilibrium. The Gibbs free energy (ΔG^0) was determined from the following relationship [25, 26]:

$$\Delta G_0 = RT \ln K_L \quad (3)$$

with R being the gas constant, K_L being equilibrium constant obtained from the Langmuir equation, and T being the absolute temperature (K). The enthalpy change (ΔH^0) and the entropy change (ΔS^0) were evaluated from Van't Hoff's equation:

$$\log K_L = \frac{\Delta S^0}{2.303R} - \frac{\Delta H^0}{2.303RT} \quad (4)$$

The values of ΔH^0 and ΔS^0 were calculated from the slope and intercept of the Van't Hoff plot of log K_L versus 1/T.

The Gibbs free energy

$$\Delta G^0 = \Delta H^0 - T\Delta S^0 \quad (5)$$

indicates the degree of spontaneity of the adsorption process, with a higher negative value reflecting a more energetically favorable adsorption process.

2.5.3 Kinetic parameters of adsorption

In order to analyze the ion adsorption kinetics onto MOCS and MOCB, three kinetic models including the pseudo-first-order equation [27], the pseudo-second-order equation [28], and the intraparticle diffusion model [29] were applied to the experimental data obtained for the time-dependent ion adsorption.

The pseudo-first-order kinetic model is given by the equation:

$$\log(q_e - q_t) = \log q_e - \frac{k_1 t}{2.303} \quad (6)$$

Similarly, the pseudo-second-order kinetic model may be written as.

$$\frac{t}{q_t} = \frac{1}{k_2 q_e^2} + \frac{t}{q_e} \quad (7)$$

while the intraparticle diffusion model may be written as:

$$qt = ktt1/2 + C \quad (8)$$

qe and qt are the amounts of solute adsorbed per unit mass of adsorbent (mmol/g) at equilibrium and at any given time t, respectively; the pseudo-first-order rate constant for the adsorption process (min^{-1}) is k_1; the rate constant for

the pseudo-second-order adsorption process [g/(mmol min)] is k_2; the initial adsorption rate for the pseudo-second order adsorption process [mmol/(g min)] is $k_2qe_2 = h$; the intraparticle diffusion rate constant [mmol/(g min)] is kt; and C is a constant. Linear plots of log(qe – qt) versus t, t/qt versus t, and qt versus t1/2 suggest the applicability of the kinetic models to the system under consideration. The kinetic parameters can be determined from the slopes and intercepts of these plots.

2.6 Determination of the activation energy

The activation energy for all considered ion adsorption was calculated via the Arrhenius Equation [26]:

$$k = k_0 \exp.(-Ea/RT) \quad (9)$$

where k is the rate constant, k_0 [g/(mmol min)] is a temperature-independent factor, Ea (J/mol) is the activation energy of the adsorption process, R is the gas constant [8.314 J/(mol K)], and T is the adsorption temperature (K). The linear form of Eq. (9) is as follows:

$$\ln k = -Ea/RT + \ln k_0 \quad (10)$$

When ln k is plotted versus 1/T, a straight line of slope –Ea/R is obtained. In our case, the rate constant under consideration was k_2, i.e., relating to the pseudo-second-order model.

3. Results and discussion

3.1 Sorbent characterization

3.1.1 SEM micrographs and EDAX spectra

To observe the morphology of the uncoated and the manganese oxide-coated sand (MOCS) and manganese oxide-coated crushed brick (MOCB), SEM micrographs were taken. Obtained results from SEM images of acid-washed uncoated sand (US) and crushed brick (UB) (**Figure 1(a)** and **(c)**) showed that the US surface was characterized by a very ordered silica crystals, and for UB it was principally a regular aluminosilicate. The surfaces of the two virgin materials seem to be uniform and smooth with small cracks and light roughness, but these manganese-oxide-coated surfaces (MOCS **Figure 1(b)**, MOCB **Figure 1(d)**) were covered by newborn manganese oxides that were certainly obtained during the coating process. **Figure 1(b)** and **(d)** also showed manganese oxides formed in clusters, apparently on occupied surfaces. The amount of manganese on the surface of the MOCS and MOCB was determined by acid digestion analysis. Results obtained for the Mn deposits were approximately 1.5 mg Mn/g for sand and 2 mg Mn/g for crushed brick. It is to note also that the quantity of manganese deposit obtained in this work for the two sorbents was found to be higher than that generally mentioned in the literature, which is about 0.003–0.5 mg Mn/g of sand [28, 30]. This reflects the effectiveness of the coating process used in this study.

The X-ray diffraction (XRD) patterns of the two coated sorbents (data not shown) revealed that the manganese oxides were amorphous, since no specific diffraction ray indicative of any specific crystalline phase was detected.

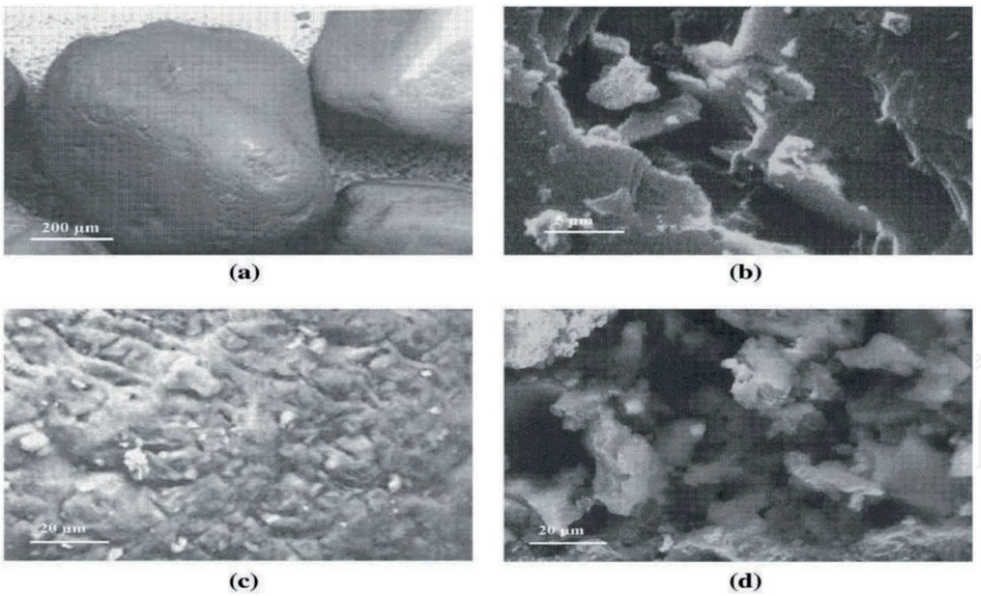

Figure 1.
SEM micrographs of samples: (a) US, (b) MOCS, (c) uncoated crushed brick, and (d) MOCB.

Figure 2(a) of the EDAX spectra of MOCS shows that Mn, O, and Si are the main constituents. These had been expected to be the principal elements of MOCS. In fact, EDAX the important peak of Si occurring in EDAX spectrum was apparently related to the too thin coating, or manganese oxides did not cover the full surface of the MOCS, allowing the X-ray to reach the sand support. From the EDAX spectrum of MOCB illustrated in **Figure 2(b)**, it was shown that Mn, O, Si, Al, Ca, and K are the dominant constituents. The presence of the Mn peak indicates the effectiveness of the adopted coating process.

3.1.2 Specific surface area

It is to note that specific surface areas of the two sorbents increased after coating. The obtained values of surface area were 1.36 and 1.86 m^2/g, for uncoated sand and uncoated crushed brick, respectively, after coating with manganese oxide the surface area of sorbents increased to 3.81 and 4.64 m^2/g, respectively. We can conclude that the addition of the manganese oxides contributes to the increase in both inner and surface porosities.

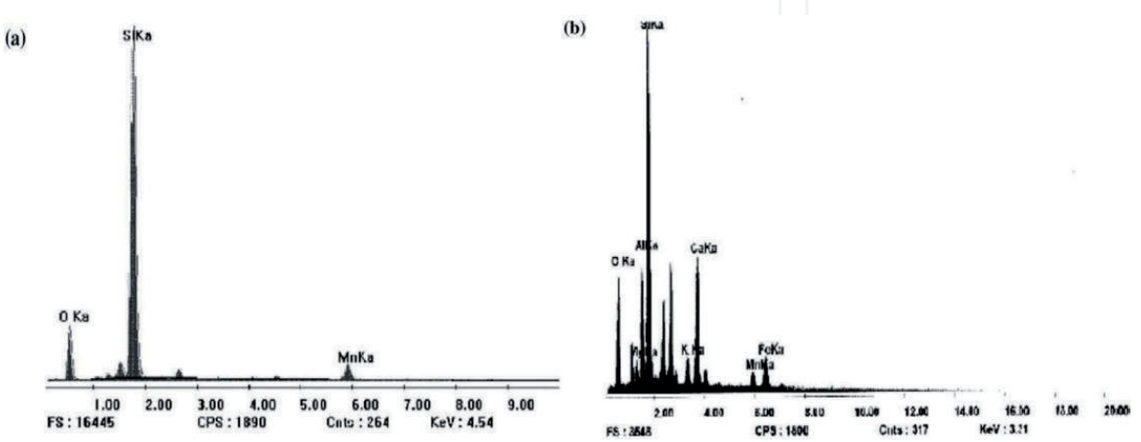

Figure 2.
EDAX spectrum of (a) MOCS and (b) MOCB.

DOI: http://dx.doi.org/10.5772/intechopen.85318

3.2 Batch adsorption experiments

3.2.1 Kinetic study

To study the effect of contact time on the sorption of all different ions, a different initial concentration was used: 10 mg/l and 50 mg/l for PO_4^{3-} and for Pb(II) and Ni(II), respectively, and a fixed pH solution of 5.0. The data showed that the sorption on MOCB and MOCS was very fast at the initial stages of the contact period, and thereafter it becomes slower near the equilibrium. The difference between the surface areas of each adsorbent can explain the differences in their sorption capacities. The sorption of all elements on the two sorbents was very fast too in the first few minutes and sharply reached a 80% removal after only 10–15 min. When the sorption process approached completion, the sorption slowed down. In this work, subsequent experiments were carried out at a contact time of 2 h for all sorbents to ensure that the equilibrium time was practically attained (**Figure 3**).

3.2.2 Effect of initial pH

Adsorption process is strongly related to pH and to the charge on both the adsorbate and the adsorbent. The surface charge on a manganese oxide surface varies with the solution pH due to the exchange of H+ ions. The surface groups on manganese oxide are amphoteric and can act as either an acid or a base. Consequently, the oxide surface can undergo protonation and deprotonation in response to changes in the solution pH [20].

The optimal pH was obtained at around pH 4. It is to note that the removal decreases continuously for pH values ranging between around 4 and 10 according to other works dealing with sorption of phosphate ions on hematite and Al_2O_3 [31], ion-exchange fiber [32], alunite [33], and bauxite [34]. The decrease in the phosphate ion uptake, occurring beyond pH 5, could be probably attributed in one hand to a competition between phosphate ions and hydroxyl ions for the sorption on the surface Lewis acid sites of the sorbent [21] and in another hand by considering a zero point of charge of the sorbent. In fact, above the zero point of charge, the positive charge density on the surface of the sorbents increases which disfavors the sorption of phosphate ions. The sorption of phosphate onto hydroxylated mineral surface can be described by a ligand exchange mechanism [35, 36], which causes an increase in pH due to the hydroxyl ions released from the oxidic sorbent. Concerning nickel sorption is negligible at the low pH values probably due to the competition effects between H_3O^+ ion and the considered species while increases progressively from pH 4. A maximum is reached at around pH 7–8; then, above pH 8 the amount of adsorbed nickel decreases as the pH increases. According to the simple species, diagrams, which were constructed for Ni(II), up to pH 8, nickel is present in the

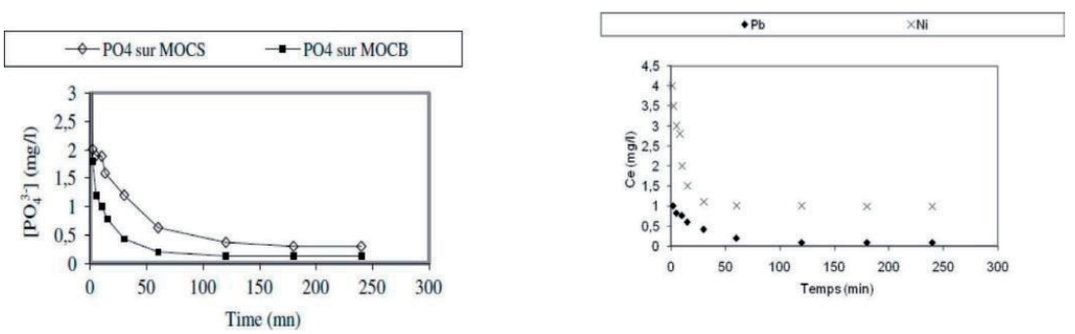

Figure 3.
Effect of contact time on all considered ions removal at pH 5 onto (a) phosphorus ions and (b) lead and nickel ions.

solution mainly in the form of Ni^{2+} ions. Neutral $Ni(OH)_2$ particles start to precipitate at pH 8 and become predominant at pH 11 [37].

The adsorption of Pb(II) ions onto both adsorbents was markedly dependent on the pH value. When the initial solution pH increased from 2 to 7, the removal of Pb (II) ion was possibly inhibited following the competition between metal ions and H+ for the available adsorption locations, while the uptake of H+ ions was more preponderant. However, the adsorption of Pb (II) ions increased with the deprotonation of the binding sites caused by the negative charge density of each adsorbent and this with the increase of the pH [20].

From our previous work [20], we have attributed this increase in adsorption with decreasing H+ ion concentration (relatively high pH values), which indicates that ion exchange is one of the major adsorption processes. Due to the equal of positive and negative groups, the total surface charge is zero, which can explain the effect of pH in terms of pHpzc value of the adsorbent. The pHpzc of MOCS and MOCB was investigated and determined to be 4.5 and 4.3, respectively [20]. If the pH was below the pHpzc, the surface charge on the adsorbent was positive; however when it is above the pHpzc value, the surface charge was negative, so the two considered adsorbents (MOCS and MOCB) have positive surface charge, and this is below the respective pH values of 4.3 and 4.5; therefore, the absorption of Pb (II) ions was low. However, the surface charges of the two adsorbents MOCS and MOCB were negative when the pH was increased above 4.3 and 4.5, respectively. The uptake is going to increase if the Pb (II) species count were either neutral or positively charged. Also, at higher pH values than pHpzc, the cation removal would be favored, and for anion, the adsorption was favored at pH values lower than pHpzc.

3.3 Sorption isotherm

The sorption of all considered ions increases as its initial concentration in the solution increases, until a maximum value (saturation state) is reached.

The maximum sorption capacity, Q_0, calculated from the Langmuir equation at 20°C, is indicated in **Table 1**.

As seen, sorption on the two coated sorbents is greater than that on virgin sand. The coatings significantly increase adsorption capacity, resulting in higher interactions between sorbents and sorbate. The values of sorption constants, derived from the Freundlich model (**Table 2**), show that the KF constant—which is a measure of sorption capacity—remains higher for MOCB than for MOCS. Values obtained of $1 < n < 10$ imply favorable sorption of all ions on the two sorbents [20, 21].

3.4 Thermodynamic adsorption parameters

Thermodynamic parameters were evaluated using the data obtained at the temperatures of 10, 20, and 40 °C. The values of ΔG0 were calculated using the

Element	SCM			BCM		
	Q_0 (mg/g)	b (l/mg)	R^2	Q_0 (mg/g)	b (l/mg)	R^2
Lead	6	2.56	0.98	6.25	3.36	0.97
Phosphate ions	1.96	0.41	0.97	2.08	1.38	0.98
Nickel	3.33	0.34	0.99	3.7	0.62	0.99

Table 1.
Langmuir parameters.

Langmuir isotherm constant, b. The values of ΔH^0 and ΔS^0 were obtained from the slope and intercept of the plot of ln b versus 1/T. **Table 3** illustrates the calculated parameters for the two adsorbents. The spontaneous nature of all ions adsorption by the two adsorbents was confirmed by the negative values of ΔG^0. On the contrary, positive values of ΔH^0 show that the adsorption process was endothermic in nature, while the positive values of ΔS^0 show the increasing randomness at solid/liquid interface during the adsorption process.

3.5 Determination of kinetic parameters

The pseudo-first-order and pseudo-second-order kinetic equations as well as the intraparticle diffusion model were applied to predict the kinetics of the adsorption of all ions onto the two adsorbents. The values, which are founded for the kinetic model, were excessively high (> 0.998); this result decreases for the intraparticle

Element	SCM			BCM		
	K_f	1/n	R^2	K_f	1/n	R^2
Lead	3.53	0.26	0.997	2.97	0.33	0.97
Phosphate ions	0.58	0.39	0.98	0.78	0.36	0.98
Nickel	0.32	0.22	0.98	0.61	0.26	0,91

Table 2.
Freundlich parameters.

Temperature (°C)			10	20	40
MOCS	Lead	ΔG° (kJ/mol)	−30.948	−32.042	−34.229
		ΔH° (kJ/mol)	42.776	42.776	42.776
		ΔS° (kJ/(kmol))	0.252	0.252	0.252
	Nickel	ΔG° (kJ/mol)	−23.35	−24.17	−25.82
		ΔH° (kJ/mol)	17.63	17.63	17.63
		ΔS° (kJ/(kmol))	0.14	0.14	0.14
	Phosphate ions	ΔG° (kJ/mol)	−24.827	−25.704	−27.459
		ΔH° (kJ/mol)	12.342	12.342	12.342
		ΔS° (kJ/(kmol))	0.129	0.129	0.129
MOCB	Lead	ΔG° (kJ/mol)	−28.432	−29.437	−31.446
		ΔH° (kJ/mol)	32.753	32.753	32.753
		ΔS° (kJ/(kmol))	0.211	0.211	0.211
	Nickel	ΔG° (kJ/mol)	−24.78	−25.68	−27.44
		ΔH° (kJ/mol)	22.78	22.78	22.78
		ΔS° (kJ/(kmol))	0.16	0.16	0.16
	Phosphate ions	ΔG° (kJ/mol)	−27.703	−28.862	−30.640
		ΔH° (kJ/mol)	24.693	24.693	24.693
		ΔS° (kJ/(kmol))	0.182	0.182	0.182

Table 3.
Thermodynamic parameters.

diffusion equation and also for the pseudo-first-order equation. Furthermore, the quantity of all considered elements adsorption at equilibrium (qe) compared to the experimental data concluded the pseudo-second-order link was more reasonable than that of the pseudo-first order model. This proposed that the removal operation move forward via a pseudo-second-order rather than a pseudo-first-order kinetic model. For this model, the initial adsorption rate, h, and the rate constant K2 diminished with the increase of the initial concentration of all considered ions; then, a limiting step may involve chemisorption [20].

4. Conclusions

Results obtained from this work showed that the deposited oxides were essentially amorphous and corresponded to 1.5 mg Mn(II)/g sand and 2 mg Mn(II)/g crushed brick.

The optimal pH adsorption for all considered ions was 5, and adsorption capacities were higher onto MOCB than MOCS.

The activation energy values for the two adsorbents found from Arrhenius plots and the kinetics which found pseudo-second order suggested that the limiting step of adsorption of all ions could be chemisorption. The results obtained in the present study suggest that manganese oxide-coated adsorbents are potentially suitable for removing of cations and anions from aqueous solution.

Author details

Nesrine Boujelben
Water Energy and Environment Laboratory, Geology Department, National Engineering School of Sfax, Sfax, Tunisia

*Address all correspondence to: nesrine.boujelben@tunet.tn

References

[1] Rao MM, Rao GPC, Seshaiah K, Choudary NV, Wang MC. Activated carbon from Ceiba pentandra hulls, an agricultural waste, as an adsorbent in the removal of lead and zinc from aqueous solutions. Waste Management (Oxford). 2008;**28**(5):849-858

[2] Liu Z, Zhong X, Wang Y, Ding Z, Wang C, Wang G, et al. An efficient adsorption of manganese oxides/activated carbon composite for lead(II) ions from aqueous solution. Arabian Journal for Science and Engineering. 2018;**43**:2155-2165

[3] Sreejalekshmi KG, Krishnan KA, Anirudhan TS. Adsorption of Pb(II) and Pb(II)-citric acid on sawdust activated carbon: Kinetic and equilibrium isotherm studies. Journal of Hazardous Materials. 2009;**161**(2-3):1506-1513

[4] Aziz HA, Adlan MN, Ariffin KS. Heavy metals (Cd, Pb, Zn, Ni, Cu and Cr(III)) removal from water in Malaysia: Post treatment by high quality limestone. Bioresource Technology. 2008;**99**(6):1578-1583

[5] Liu YX, Yan JM, Yuan DX, Li QL, Wu XY. The study of lead removal from aqueous solution using an electrochemical method with a stainless steel net electrode coated with single wall carbon nanotubes. Chemical Engineering Journal. 2013;**218**:81-88

[6] Al-Othman ZA, Naushad Inamuddin M. Organic–inorganic type composite cation exchanger poly-o-toluidine Zr(IV) tungstate: Preparation, physicochemical characterization and its analytical application in separation of heavy metals. Chemical Engineering Journal. 2011;**172**(1):369-375

[7] O'Connell DW, Birkinshaw C, O'Dwyer TF. Heavy metal adsorbents prepared from the modification of cellulose: A review. Bioresource Technology. 2008;**99**:6709-6724

[8] Mohan D, Singh KP. Single- and multi-component adsorption of cadmium and zinc using activated carbon derived from bagasse—An agricultural waste. Water Research. 2002;**36**(9):2304-2318

[9] Han RP, Zhu L, Zou WH, Wang DT, Shi J, Yang JJ. Removal of copper(II) and lead(II) from aqueous solution by manganese oxide coated sand—II. Equilibrium study and competitive adsorption. Journal of Hazardous Materials. 2006;**137**(1):480-488

[10] Ghaedi M, Biyareh MN, Kokhdan SN, Shamsaldini S, Sahraei R, Daneshfar A, et al. Comparison of the efficiency of palladium and silver nanoparticles loaded on activated carbon and zinc oxide nanorods loaded on activated carbon as new adsorbents for removal of Congo red from aqueous solution: Kinetic and isotherm study. Materials Science and Engineering: C. 2012;**32**(4):725-734

[11] Sun YB, Yang SB, Chen Y, Ding CC, Cheng WC, Wang XK. Adsorption and desorption of U(VI) on functionalized graphene oxides: A combined experimental and theoretical study. Environmental Science & Technology. 2015;**49**:4255-4262

[12] Ma MH, Gao HY, Sun YB, Huang MS. The adsorption and desorption of Ni(II) on Al substituted goethite. Journal of Molecular Liquids. 2015;**201**:30-35. International Journal of Environmental Research Public Health. 2017, 14, 1145 10 of 11

[13] Sounthararajah DP, Loganathan P, Kandasamy J, Vigneswaran S. Effects of humic acid and suspended solids on the removal of heavy metals from water by adsorption onto granular activated carbon. International Journal of Environmental Research and Public Health. 2015;**12**:10475-10489

[14] Lee SM, Laldawngliana C, Tiwari D. Iron oxide nano-particles-immobilized-sand material in the treatment of Cu(II), Cd(II) and Pb(II) contaminated waste waters. Chemical Engineering Journal. 2012;**195**:103-111

[15] Tani Y, Miyata N, Ohashi M, Ohnuki T, Seyama H, Iwahori K, et al. Interaction of inorganic arsenic with biogenic manganese oxide produced by a Mn-oxidizing fungus, strain KR21-2. Environmental Science & Technology. 2004;**38**:6618-6624

[16] Kennedy C, Smith DS, Warren LA. Surface chemistry and relative Ni sorptive capacities of synthetic hydrous Mn oxyhydroxides under variable wetting and drying regimes. Geochimica et Cosmochimica Acta. 2004;**68**:443-454

[17] Villalobos M, Bargar J, Sposito G. Mechanisms of Pb(II) sorption on a biogenic manganese oxide. Environmental Science & Technology. 2005;**39**:569-576

[18] Benjamin MM, Slatten RS, Bailey RP, Bennett T. Sorption and filtration of metals using iron oxide coated sand. Water Research. 1996;**30**:2609-2620

[19] Sharma SK, Petrusevski B, Schippers JC. Characterisation of coated sand from iron removal plants. Journal of Water Supply: Research and Technology. 2002;**2**:247-257

[20] Boujeben N, Bouzid J, Elouear Z. Removal of Lead(II) ions from aqueous solutions using manganese oxide-coated adsorbents: Characterization and kinetic study. Adsorption Science & Technology. 2009;**27**:2

[21] Boujelben N, Bouhamed F, Elouear Z, Bouzid J, Feki M. Removal of phosphorus ions from aqueous solutions using manganese-oxide-coated sand and brick. Desalination and Water Treatment. 2014;**52**:2282-2292

[22] Bajpai S, Chaudhuri M. Removal of arsenic from ground water by manganese dioxide–coated sand. Journal of Environmental Engineering. 1999;**125**(8):782-784

[23] Lo SL, Jengh T, Lai CH. Characteristics and adsorption properties of an ironcoated sand. Water Science and Technology. 1997;**35**:63-70

[24] Seader JD, Herley EJ. Separation Process Principles. New York: Wiley; 1998

[25] Aksu Z. Determination of the equilibrium, kinetic and thermodynamic parameters of the batch biosorption of nickel (II) ions onto chlorella vulgaris. Process Biochemistry. 2002;**38**(1):89-99

[26] Namasivayam C, Ranganathan K. Waste Fe(III)/Cr(III) hydroxide as adsorbent for the removal of Cr(VI) from aqueous solution and chromium plating industry waste water. Environmental Pollution. 1993;**82**:255-261

[27] Panday KK, Prasad G, Singh VN. Copper(II) removal from aqueous solutions by fly ash. Water Research. 1985;**19**:869-873

[28] Selvaraj R, Younghun K, Cheol KJ. Removal of copper from aqueous solution by aminated and protonated mesoporous aluminas: Kinetics and equilibrium. Journal of Colloid and Interface Science. 2004;**273**:14-21

[29] Chiron N, Guilet R, Deydier E. Adsorption of Cu(II) and Pb(II) onto a grafted silica: Isotherms and kinetic models. Water Research. 2003;**37**(13):3079-3086

[30] Chang YY, Kim KS, Jung JH, Yang JK, Lee SM. Application of iron-coated sand and manganese-coated sand on the treatment of both As(III) and

As(V). Water Science and Technology. 2007;**55**:69-75

[31] Hu P-Y, Hsieh Y-H, Chen J-C, Chang C-Y. Characteristics of manganese-coated sand using SEM and EDAX analysis. Journal of Colloid and Interface Science. 2004;**274**:308-312

[32] Horanyi G, Joo P. Some peculiarities in the specific adsorption of phosphate ions on hematite c-Al_2O_3 as reflected by radiotracer studies. Journal of Colloid and Interface Science. 2002;**247**:12-17

[33] Xia LR, Jinlong G, Hongxiao T. Adsorption of fluoride, phosphate, and arsenate ions on a new type of ion exchange fiber. Journal of Colloid and Interface Science. 2002;**248**:268-274

[34] Ozacar M. Phosphate adsorption characteristics of alunite to be used as a cement additive. Cement and Concrete Research. 2003;**2372**:1-5

[35] Altundogan HS, Tumen F. Removal of phosphates from aqueous solutions by using bauxite. I: Effect of pH on the adsorption of various phosphates. Journal of Chemical Technology & Biotechnology. 2001;**77**:77-85

[36] Goldberg S, Sposito G. On the mechanism of specific phosphate adsorption by hydroxylated mineral surfaces: A review. Communications in Soil Science and Plant Analysis. 1985;**16**:801-821

[37] Mavros P, Zouboulis AI, Lazaridis NK. Removal of metal ions from wastewaters the case of nickel. Journal of Environmental Technology. 1993;**14**:83-91